Intermolecular Structure and Thermodynamics of Vinyl Polymer Liquids: Freely-Jointed Chains†

John G. Curro

Sandia National Laboratories, Albuquerque, New Mexico 87185

Received February 15, 1994; Revised Manuscript Received May 9, 1994®

ABSTRACT: Polymer reference interaction site model (RISM) calculations are performed on melts of freely-jointed, vinyl polymer chains. The local monomer structure is modeled by three independent, hard-sphere sites corresponding to the CH_2 and CH backbone constituents and an arbitrary side-chain group. The six intersite radial distribution functions and partial structure factors are computed for chains of 100 backbone units, at a liquidlike packing fraction of 0.5. It is found that the side-chain groups tend to shield the backbone sites from approaching each other at short distances. The extent of shielding increases with the size of the side-chain group. On a radius of gyration length scale all the radial distribution functions exhibit a universal correlation hole. The total structure factor, proportional to the intensity of scattering, exhibits a low-angle peak not present in a polyethylene-like melt. This low-angle peak grows in intensity and shifts to lower wave vectors as the size of the side-chain moiety increases. The isothermal compressibility, equation-of-state, and cohesive energy of the liquid are found to be functions of the local monomer structure.

I. Introduction

Over the past several years Curro and Schweizer have developed[1-3] a computationally tractable, statistical mechanical theory for the intermolecular structure and thermodynamics of polymer liquids. This approach is an extension to flexible polymers of the *reference interaction site model* or RISM theory of Chandler and Andersen[4,5] successfully used to study small, rigid molecule fluids.[6,7] The polymer RISM or PRISM theory has been used to treat linear, freely-jointed,[8,9] semiflexible,[10] rotational isomeric state,[11,12] and threadlike[13] chains. In addition, several investigators have applied PRISM theory to study polymer alloys.[14-16] In all of these PRISM computations, each polymer molecule is represented as a chain containing a single type of site. Recently, David and Schweizer[17] used a two-site chain model to represent block copolymers.

In the present investigation we apply PRISM theory to study the structure of freely-jointed vinyl polymer melts using a three-site model according to $-(ABC)_n-$ where A and B represent backbone sites and C represents the side group. The added mathematical complexity of including three rather than a single distinct site would appear to be necessary to capture the details of the local intermolecular packing of vinyl polymers in the liquid. The long-range part of the radial distribution function $g(r)$, the so-called correlation hole regime, would be expected to be insensitive to whether a three- or one-site model is employed as long as the radius of gyration is the same.[8,13] On the other hand, the thermodynamic properties of the liquid would be expected to depend on the local packing since van der Waals attractions, known to significantly contribute to the thermodynamics, are short range. Thus the level of local chemical detail necessary depends on the questions one is addressing.

Here we will examine how the side group influences the intermolecular packing by studying the radial distribution functions, structure factors, and equation-of-state as a function the size of the side group represented by the C site. In this investigation we will focus only on freely-jointed vinyl chains. For calculations on specific vinyl polymer melts one needs to include the effects of constant bond angles and rotational potentials.

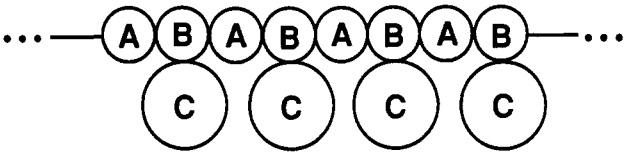

Figure 1. Schematic representation of the freely-jointed polymer chain used in this investigation. Each monomer is composed of three independent, tangent, hard-sphere sites.

In section II the PRISM theory is recast in a form appropriate for chains of three independent sites. The intramolecular structure factors of freely-jointed vinyl chains, needed as input for the PRISM theory, are developed in section III. In section IV the intermolecular radial distribution functions and structure factors calculated from the PRISM theory are discussed. Finally, in section VI the equation-of-state and cohesive energy are calculated for freely-jointed vinyl chain liquids.

II. PRISM Theory

Consider a system consisting of N_c polymer chains each containing N monomers. Each monomer is made up of one or more interaction sites. In the vinyl polymer case considered here, each monomer consists of three independent species sites (A, B, C) corresponding to the CH_2, CH, and R moieties making up the backbone of a vinyl polymer $-(CH_2CHR)_N-$. Figure 1 depicts the arrangement of the sites along the chain backbone. Although it is not necessary in general, in the present investigation we take the sites to consist of tangent hard spheres as illustrated in Figure 1. We now label the sites on each molecule from 1 to $3N$ and define an intermolecular site–site radial distribution function matrix $g_{\alpha\gamma}(r)$ according to[5]

$$\rho^2 g_{\alpha\gamma}(r) = \langle \sum_{i\neq j=1}^{N_c} \delta(\vec{r}_i^{\,\alpha})\, \delta(\vec{r}-\vec{r}_j^{\,\gamma}) \rangle \qquad (1)$$

where $\rho = N_c/V$ is the number density of molecules and $\vec{r}_i^{\,\alpha}$ is the position vector of site α on chain i. Strictly speaking $g_{\alpha\gamma}(r)$ is a $3N \times 3N$ matrix since each site along the chain would be distinct in the general case.

It is convenient to define the total correlation function $h_{\alpha\gamma}(r) = g_{\alpha\gamma}(r) - 1$ so that $h(r)$ approaches zero as r becomes

† This work performed at Sandia National Laboratories supported by the U.S. Department of Energy under Contract No. DE-AC04-76DP00789.

® Abstract published in *Advance ACS Abstracts*, July 15, 1994.

0024-9297/94/2227-4665$04.50/0

large. Following Chandler and Andersen, we now define the direct correlation function $C_{\alpha\gamma}(r)$ from a generalized Ornstein–Zernike equation[4,5] written below in Fourier space.

$$\hat{\mathbf{h}}(k) = \hat{\omega}(k)\cdot\hat{\mathbf{C}}(k)\cdot[\hat{\omega}(k) + \rho\hat{\mathbf{h}}(k)] \tag{2}$$

In eq 2 $\mathbf{h}(r)$, $\mathbf{C}(r)$, and $\omega(r)$ are $3N \times 3N$ matrices with elements $h_{\alpha\gamma}$, $C_{\alpha\gamma}$, and $\omega_{\alpha\gamma}$, and the caret denotes Fourier transformation with wave vector k. The normalized intramolecular distribution between intramolecular sites α and γ is denoted by $\omega_{\alpha\gamma}(r)$. Equation 2 can be viewed as a definition of the direct correlation functions $\mathbf{C}(r)$. To have a soluble system of equations, Chandler and Andersen[4,5] proposed that the direct correlation functions be approximated by the Percus–Yevick closure in analogy with the Percus–Yevick theory (PY) of atomic liquids. For hard-core potentials the PY closure has the simple form

$$g_{\alpha\gamma}(r) = 0 \qquad r < d_{\alpha\gamma}$$

$$C_{\alpha\gamma}(r) \cong 0 \qquad r > d_{\alpha\gamma} \tag{3}$$

where $d_{\alpha\gamma}$ is the hard-core distance between sites α and γ along the chain. Equations 2 and 3 make up the RISM theory of Chandler and Andersen.

Equations 2 and 3 do not yield a tractable theory for polymer liquids since one is confronted with solving $3N(3N + 1)/2$ independent equations where N, the number of monomers, is a large number ($N \gg 1$). This difficulty is easily dealt with by recognizing that, since the polymer chains are long, we can neglect end effects.[1-3] Such an approximation implies that we can treat each of the N monomers as being equivalent. Since each monomer contains three species sites, we have only six independent radial distribution functions and direct correlation functions

$$h_{\alpha\gamma}(r) = h_{mm'}(r); \quad C_{\alpha\gamma}(r) = C_{mm'}(r) \tag{4}$$

where $\alpha \in m$, $\gamma \in m'$, and m and m' take on the species labels A, B, and C. Thus the $3N \times 3N$ matrices in eq 2 are made up of blocks of identical 3×3 symmetric matrices, where each block consists of correlation functions between species, i.e., h_{AA}, h_{BB}, h_{CC}, h_{AB}, h_{AC}, and h_{BC}. Using eq 4 in eq 2 gives

$$\hat{h}_{mm'}(k) = \sum_{m''m'''} \hat{C}_{m''m'''}\Bigg[\sum_{\lambda\in m''}\hat{\omega}_{m\lambda}\sum_{\sigma\in m''}\hat{\omega}_{\sigma m'} + \frac{1}{2}\rho N_{m''}\hat{h}_{m''m'}\sum_{\lambda\in m'''}\hat{\omega}_{m\lambda} + \frac{1}{2}\rho N_{m'''}\hat{h}_{m'''m'}\sum_{\lambda\in m''}\hat{\omega}_{m\lambda}\Bigg] \tag{5}$$

where the Greek indices get summed over the $3N$ total number of sites, but the indices denoted by m, m', etc., refer to the species A, B, or C. For a vinyl chain of N monomers, we have exactly N sites each of species A, B, and C. We now define a symmetric, 3×3, intramolecular structure factor matrix based on species according to

$$\hat{\Omega}_{mm'}(k) = \frac{1}{N}\sum_{\lambda\in m}\sum_{\sigma\in m'}\hat{\omega}_{\lambda\sigma}(k) \tag{6}$$

With this definition eq 5 can be written in the compact form

$$\hat{\mathbf{h}}(K) = \hat{\Omega}(k)\cdot\hat{\mathbf{C}}(K)\cdot[\hat{\Omega}(k) + \tilde{\rho}\hat{\mathbf{h}}(k)] \tag{7}$$

where $\tilde{\rho} = N\rho$ is the monomer density and $h_{mm'}(r)$ and $C_{mm'}(r)$ are symmetric 3×3 matrices involving pairs of sites of species A, B, and C. From eq 7 we see that polymer RISM theory for the vinyl polymer liquid reduces to a set of six independent equations for the various radial distributions $g_{AA}(r)$, $g_{BB}(r)$, $g_{CC}(r)$, $g_{AB}(r)$, $g_{AC}(r)$, and $g_{BC}(r)$ of interest. The PRISM equations in eq 7 are to be used with the analogous PY closure for hard-core interactions.

$$g_{mm'}(r) = 0 \qquad \text{for } r < d_{mm'}$$

$$C_{mm'}(r) = 0 \qquad \text{for } r > d_{mm'} \tag{8}$$

In the RISM theory of rigid molecules the intramolecular distributions $\omega_{\alpha\gamma}(r)$ are well-defined and serve to specify the positions of the sites on the rigid molecule. In the case of a flexible polymer liquid, where the molecules have a large number of internal degrees of freedom, one might expect that the intramolecular functions $\omega_{\alpha\gamma}(r)$ would have to be determined self-consistently with the intermolecular structure given by the $h(r)$'s. We can circumvent this difficulty, at least to a first approximation, by making use of Flory's hypothesis[18] that polymer chains in a melt are ideal. It has been demonstrated by neutron scattering experiments[19,20] and computer simulations[21,22] that, to a good approximation, intramolecular excluded-volume interactions are screened out in a melt. This allows us to considerably simplify the problem by calculating the $\hat{\Omega}_{mm'}(k)$ in eq 6 using the average values of $\hat{\omega}_{\alpha\gamma}(k)$ from a separate single-chain calculation, appropriate to the particular model chain of interest. The ideality hypothesis is not strictly valid on monomer length scales for completely flexible polymers. Recent computer simulations[9] of Grest and Kremer indicate that, although the chains in the melt scale as ideal chains (i.e., $R_G \sim \sqrt{N}$), some local expansion of the chains relative to an ideal state occurs. These intramolecular expansion effects are expected to become less important as the chains become stiffer and are not as important in most real polymers. Methods have been developed to include these intramolecular expansion effects in a self-consistent manner.[10,23-27] Such intramolecular expansion effects are beyond the scope of the present investigation on vinyl polymers.

III. Intramolecular Structure

In the first application of PRISM theory to vinyl polymers presented here, we will make use of the freely-jointed chain model for the intramolecular structure of the polymers. In the standard linear freely-jointed model the chain is divided into equal segments with the angle between adjacent segments free to assume any value with equal probability. For the vinyl polymer we will adopt this model for the alternating segments joining AB and BA site pairs along the chain backbone. In addition, we take each segment (BC) joining the side group to the main chain to also be freely jointed and free to rotate. For such a model we can then write the intramolecular structure factor of eq 6 in the form

$$\hat{\Omega}_{mm'}(k) = \frac{1}{N}\sum_{\lambda\in m}\sum_{\sigma\in m'}\left[\frac{\sin(kd_{mm'})}{kd_{mm'}}\right]^{n(\lambda,\sigma)} \tag{9}$$

where $n(\lambda,\sigma)$ is the number of chain segments between a pair of sites λ and σ along the chain backbone depicted in Figure 1. The term in square brackets arises from the constant bond length constraint for freely-jointed chains.[28] Although the calculation is somewhat tedious, the sum-

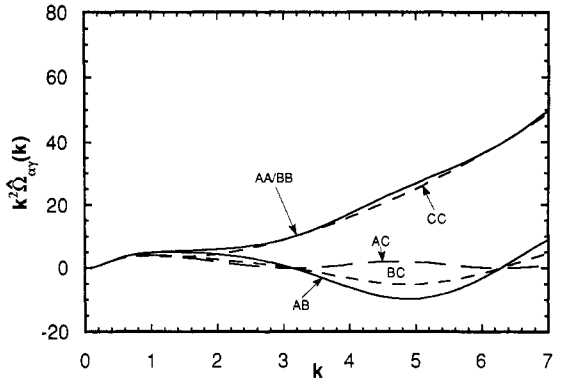

Figure 2. Kratky plot of the intramolecular structure functions $\hat{\Omega}_{\alpha\gamma}(k)$ calculated from eq 10 as a function of wave vector k (Å^{-1}). The number of monomer units N was taken to be 50.

mations in eq 9 can be performed analytically to give

$$\hat{\Omega}_{AA}(k) = \hat{\Omega}_{BB}(k) = \frac{[N - Nf_{AB}^4 - 2f_{AB}^2 + 2f_{AB}^{2(N+1)}]}{N(1-f_{AB}^2)^2} \quad (10a)$$

$$\hat{\Omega}_{CC}(k) = \frac{f_{BC}^2[N - Nf_{AB}^4 - 2f_{AB}^2 + 2f_{AB}^{2(N+1)}]}{N(1-f_{AB}^2)^2} + (1-f_{BC}^2) \quad (10b)$$

$$\hat{\Omega}_{AB}(k) = \frac{f_{AB}[2N - 1 - (2N+1)f_{AB}^2 + f_{AB}^{2N} + f_{AB}^{2(N+1)}]}{N(1-f_{AB}^2)^2} \quad (10c)$$

$$\hat{\Omega}_{AC}(k) = f_{BC}\hat{\Omega}_{AB}(k); \quad \hat{\Omega}_{BC}(k) = f_{BC}\hat{\Omega}_{BB}(k) \quad (10d)$$

In eq 10 f_{AB} and f_{BC} are defined as

$$f_{AB} = \frac{\sin(kd_{AB})}{kd_{AB}} \quad \text{and} \quad f_{BC} = \frac{\sin(kd_{BC})}{kd_{BC}} \quad (10e)$$

Equation 10 can be used in the PRISM eq 7 along with the closures in eq 8 to calculate the six radial distribution functions between species sites at any given monomer density $\tilde{\rho}$.

In Figure 2 a Kratky plot is shown for the various intramolecular structure factors calculated according to eqs 10 for vinyl chains of $N = 50$ monomers where all three sites are the same size $d_{AA} = d_{BB} = d_{CC} = 1.0$ Å. Note that the diagonal components of $\hat{\Omega}(k)$ show a well-defined plateau or intermediate scaling regime. The shape of the diagonal components on the Kratky plot is very similar to what is observed[8,9] in freely-jointed polymer melts consisting of a single site. The off-diagonal components, however, exhibit different behavior at higher wave vectors and become negative in certain wave vector regimes.

In this investigation we want to examine trends in the radial distribution functions as the size of the side group site C is changed. In order to make a sensible comparison, it is necessary to keep the packing fraction η of sites fixed in each calculation. Since we are using an intramolecular chain model that is ideal and hence allows unphysical overlaps of intramolecular sites, the average packing fraction depends not only on the monomer density but also the degree of polymerization N and the sizes of the individual sites. As in the case of the local self-consistency problem discussed above, this unphysical chain overlap has been found to decrease substantially when we consider real chains that have stiffness.

Table 1. Overlap Fraction Δ Shown for Chains of $N = 50$, $d_{AA} = d_{BB} = 1.0$ Å for Various Values of d_{CC}[a]

d_{CC} (Å)	Δ	$\tilde{\rho}$ (Å^{-3})	d_{CC} (Å)	Δ	$\tilde{\rho}$ (Å^{-3})
0	0.175	0.579	1.0	0.231	0.414
0.2	0.176	0.577	1.2	0.261	0.347
0.4	0.183	0.566	1.4	0.301	0.288
0.6	0.198	0.537	1.5	0.323	0.262
0.8	0.214	0.484			

For the completely flexible, freely-jointed chain, however, we must deal with this untidy problem. In previous studies[8,10] on freely-jointed chains consisting of a single independent site, we corrected for this effect by assuming pairwise additivity of intramolecular overlaps. Here we will adopt this scheme to estimate the overlap fraction Δ of freely-jointed vinyl chains. For vinyl chains the packing fraction is related to the monomer density by

$$\eta = \left[\frac{\pi(d_{AA}^3 + d_{BB}^3 + d_{CC}^3)}{6}\right]\tilde{\rho}(1-\Delta) \quad (11)$$

where Δ is approximated by assuming pairwise additivity of intramolecular overlaps

$$\Delta \cong \left[\frac{6}{\pi N(d_{AA}^3 + d_{BB}^3 + d_{CC}^3)}\right]\sum_{\alpha\gamma}\int_0^{d_{\alpha\gamma}} d\vec{r}\ \omega_{\alpha\gamma}(r)\ V_{\alpha\gamma}(r) \quad (12)$$

In eq 12 $\omega_{\alpha\gamma}(r)$ is the normalized probability between sites α and γ for a freely-jointed vinyl chain, and $V_{\alpha\gamma}(r)$ is the overlap volume between two spheres a distance r apart having diameters $d_{\alpha\alpha}$ and $d_{\gamma\gamma}$. The details of computing Δ are shown in the Appendix. Table 1 gives the overlap fraction for a freely-jointed vinyl chain of $N = 50$ monomer units as a function of the size d_{CC} of the side group C.

IV. Intermolecular Structure

In this investigation we study the intermolecular structure of vinyl polymer liquids having 50 monomer units (100 backbone sites) at a liquidlike packing fraction of 0.5. To calculate the intermolecular packing, we solve the PRISM equations in eq 7 numerically for hard-core interactions between A, B, and C sites using the closure in eq 8. In this work we choose the backbone site diameters to be equal to 1 Å for convenience. Alternatively, the distance r and wave vector k can be considered to be nondimensionalized by the backbone site diameter (i.e., r/d_{AA} and kd_{AA}).

The numerical problem involves solving six coupled, nonlinear integral equations that we solve using standard Picard iteration.[29] The procedure starts by assuming $\gamma(r) = \mathbf{h}(r) - \mathbf{C}(r)$ at (usually $2^{11} = 2048$) equally spaced points in r space ($\Delta r = 0.04$). The closure condition in eq 8 is then used to compute $\mathbf{C}(r)$ from $\gamma(r)$, which is then fast Fourier transformed to yield $\hat{\mathbf{C}}(k)$ at 2048 equally spaced intervals in k space ($\Delta k = \pi/(2048)(0.04) = 0.038\,349\,5$). The PRISM matrix equations in eq 7 are then solved numerically to give a new estimate

$$\hat{\gamma}(k) = [1 - \tilde{\rho}\hat{\Omega}(k)\cdot\hat{\mathbf{C}}(k)]^{-1}\cdot\hat{\Omega}(k)\cdot\hat{\mathbf{C}}(k)\cdot\hat{\Omega}(k) - \hat{\mathbf{C}}(k) \quad (13)$$

After carrying out another fast Fourier transform back to r space, the new $\gamma(r)$ is compared with the previous estimate. A solution is assumed when the average fractional difference between estimates is less than 10^{-7}. If convergence is not obtained, the above procedure is repeated using a new guess for $\gamma(r)$. The new guess is constructed by mixing 5–10% of the latest $\gamma(r)$ with 90–

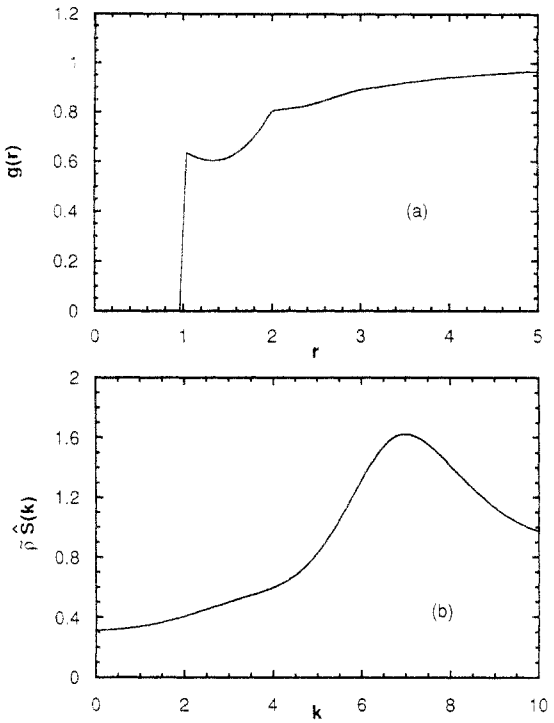

Figure 3. Intermolecular structure calculated for a polyethylene type melt of chains containing 100 backbone repeat units (50 monomers) of size d = 1.0 Å. (a) Radial distribution function $g(r)$ as a function of r (Å). (b) Structure factor $\hat{S}(k)$ as a function of wave vector k (Å^{-1}).

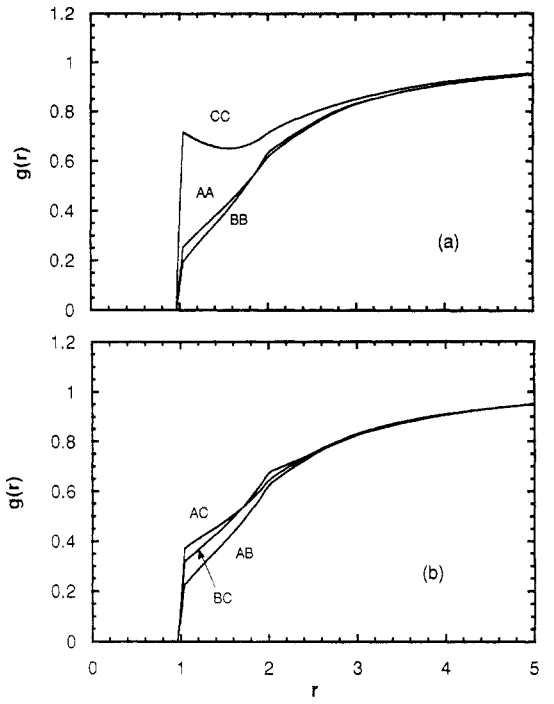

Figure 4. Intermolecular radial distribution functions for a freely-joined melt of N = 50 monomers (100 backbone sites) as a function of r (Å). The site diameters are $d_{AA} = d_{BB} = d_{CC}$ = 1.0 Å. (a) Radial distribution functions between sites of the same type as a function of r (Å). (b) Radial distribution functions between sites of different types as a function of r (Å).

95% of the previous estimate. Depending on how good the initial guess is, the process usually converges after several hundred iteration cycles. Generally, it was found prudent to use the best guess available for $\gamma(r)$, for example, from a previous successful run with similar parameters. In order to obtain a first guess, the solution from the corresponding one-site model was used. The results were found not to change significantly when the number of mesh points was changed from 2048 to 4096.

The intramolecular structure is entirely specified by the intramolecular structure factor matrix $\hat{\Omega}(k)$ in eq 13. For freely-jointed vinyl chains studied here eqs 10 were used for this purpose. Typical results for these intramolecular structure functions are shown in Figure 2.

It is instructive to compare the three-site vinyl polymer melt with the corresponding one-site model of a polyethylene (PE) type chain liquid at the same packing fraction. The intermolecular radial distribution function $g(r)$ of such a freely-jointed PE chain melt is shown in Figure 3a. Note that $g(r)$ is zero inside the hard core ($r < d$ = 1.0 Å) and then jumps discontinuously at $r = d$. The cusp at $r = 2d$ is a consequence of the tangent hard-sphere model with a constant bond constraint. One can clearly observe the *correlation hole* where $g(r)$ monotonically approaches 1 on a scale of the radius of gyration (R_g = 4.08 Å). The correlation hole[30] is a consequence of the screening of a pair of intermolecular sites on two chains by the remaining intramolecular sites.

Figure 4 depicts the intermolecular radial distribution functions for a vinyl polymer liquid with the sizes of the three sites equal ($d_{AA} = d_{BB} = d_{CC}$ = 1.0 Å). A prominent characteristic of vinyl polymer liquids that can be deduced from this figure is that the side group site tends to screen out the backbone sites at short distances. Comparison of Figures 3a and 4a indicates that $g_{CC}(r)$ is larger near contact than $g(r)$ for the corresponding PE type chain. This is undoubtedly a consequence of the fact that the C sites are side groups off the backbone and, therefore, are more accessible to each other than backbone sites. These side-chain sites effectively shield the backbone sites A and B from each other at short distances. This is evident from Figure 4a since $g_{AA}(r)$ and $g_{BB}(r)$ are much smaller than $g_{CC}(r)$ near contact. Note that $g_{AA}(r)$ is slightly larger than $g_{BB}(r)$ since site C has a greater shielding effect on B (since it is directly attached) than on site A. Figure 4b depicts the radial distribution functions between unlike types of sites. Again, the relative magnitudes near contact are explainable by side-group shielding arguments.

It is interesting to also examine the radial distributions in Figure 4 on long length scales. It can be seen that, in the correlation hole regime, all the intersite $g(r)$'s are essentially the same as for the corresponding PE type melt. This universal behavior is not surprising since the structural differences between a vinyl and a PE type polymer occur only at the monomer level. These local structural features will, in general, affect the radius of gyration and thereby indirectly influence the correlation hole. However, since both chains are ideal, freely-jointed chains with the same number of backbone segments, their radii of gyration will be identical in this case. From these considerations, it would appear that a coarse-grained model chain effectively captures the correlation hole features of a polymer liquid, as long as the radius of gyration matches that of the real chain. The short-range structural features depend on the details of the monomer structure as is clearly seen in Figure 4.

We will now examine the effect of the size of the side-chain substituent on the intermolecular packing in the vinyl polymer melt. Figure 5 displays the intermolecular radial distribution $g_{AA}(r)$ between backbone sites of type A as a function of the diameter d_{CC} of the side chain site C. Here we observe an interesting nonmonotonic behavior for side-chain groups of small size. When d_{CC} is zero, we of course reduce to the PE case shown in Figure 3a. Three d_{CC}'s were studied (0, 0.2, and 0.4 Å) in the range $0 \le d_{CC} \le 0.4$ Å. In all three cases the $g_{AA}(r)$'s found were

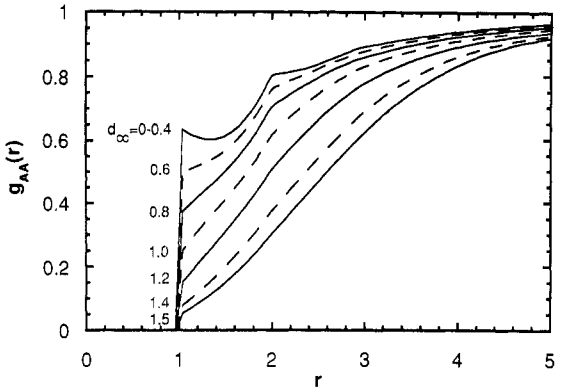

Figure 5. Intermolecular radial distribution function $g_{AA}(r)$ between backbone sites of type A, for various values of the side-chain site diameter d_{CC} (Å), as a function of r (Å). The backbone site diameters were $d_{AA} = d_{BB} = 1.0$ Å.

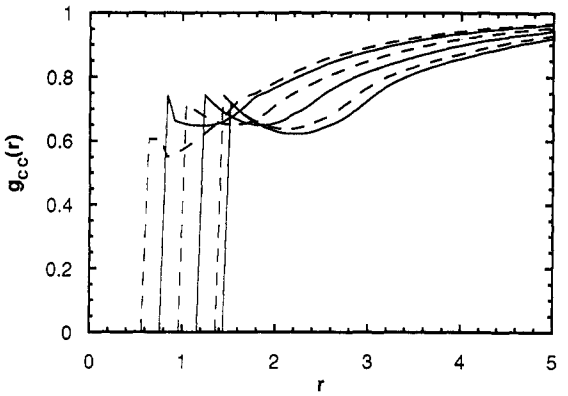

Figure 6. Intermolecular radial distribution function $g_{CC}(r)$ between backbone sites of type C, for various values of the side-chain site diameter d_{CC} (Å), as a function of r (Å). The backbone site diameters were $d_{AA} = d_{BB} = 1.0$ Å.

approximately the same as $g(r)$ shown in Figure 3a for PE type melts.

We can speculate that $g_{AA}(r)$ remains unaffected by the side-chain site in this region because of preferred packing arrangements. When site C is in the range $0 \le d_{CC} \le 0.4$ Å, the extra volume associated with the side group can be accommodated into the normal PE type packing by filling interstitial sites in the amorphous liquid. This is supported by the fact that the maximum diameter sphere that can be fit in the space between four touching spheres of diameter d, lying in the same plane, is $0.414d$. Such preferred packing arrangements, if they occur, would be greatly facilitated in the freely-jointed vinyl chains studied here. This is further supported by the fact that Picard iteration tended to give unphysical numerical results for the $g_{CC}(r)$ in which $g_{CC}(r)$ became negative near contact when $0 \le d_{CC} \le 0.4$ Å. Such unphysical behavior for $g_{CC}(r)$ might suggest that the C sites are being surrounded by backbone sites and are impeded from coming in contact with each other. Because of free rotation of the angle joining adjacent sites ABC, the side group could rotate into the space between four backbone sites. For this reason the nonmonotonic behavior observed here for freely-jointed chains would probably not occur with more realistic models of vinyl chains having fixed bond angles.

For $d_{CC} > 0.4$ Å we observe in Figure 5 that the shielding effect of the side group increases as its size increases. In contrast to what was found for small d_{CC}, the Picard iteration scheme yielded physically meaningful solutions for $g_{CC}(r)$ in which $g_{CC}(r)$ remains positive outside the hard core. In Figure 6 we have plotted $g_{CC}(r)$ for various values of d_{CC}. It can be seen from this figure that $g_{CC}(r)$ near contact remains fairly constant for $d_{CC} > 0.6$ Å.

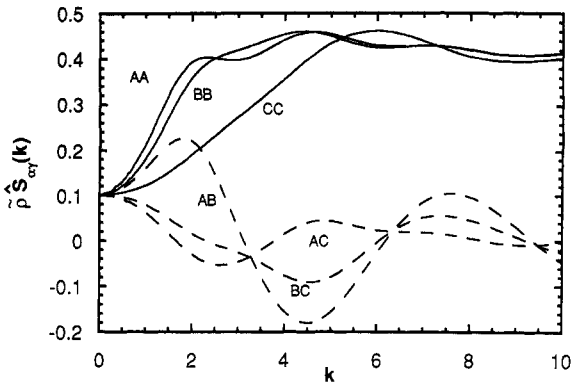

Figure 7. Partial structure factors calculated from Eq 14b as a function of wave vector k (Å^{-1}). The backbone site diameters were $d_{AA} = d_{BB} = d_{CC} = 1.0$ Å.

We now examine the scattering behavior of freely-jointed polymer melts. A structure factor matrix can be defined[15] in terms of the intramolecular and intermolecular structure.

$$\hat{\mathbf{S}}(k) = \hat{\Omega}(k) + \tilde{\rho}\hat{\mathbf{h}}(k) \tag{14a}$$

$$\hat{\mathbf{S}}(k) = [1 - \tilde{\rho}\hat{\Omega}(k)\cdot\hat{\mathbf{C}}(k)]^{-1}\cdot\hat{\Omega}(k) \tag{14b}$$

The second relation in eq 14 follows from the PRISM matrix equations in eq 7. From a numerical standpoint, it was found that better accuracy could be obtained by computing the structure factors from the direct correlation functions rather than from the functions $\hat{\mathbf{h}}(k)$. For this reason eq 14b was employed to calculate the partial structure factors in this work.

It is instructive to first examine the structure factor for a single-site PE type polymer melt. This structure factor is plotted in Figure 3b for freely-jointed chain melts having a site diameter of 1 Å. The single feature evident in this figure is the peak occurring at $k_1 \cong 7$ Å^{-1}. This peak roughly corresponds to a distance $2\pi/k_1 \cong 1$ and results from both intramolecular, site–site bonds and intermolecular, site–site bonds and intermolecular, nearest-neighbor packing. This first peak is seen at $k_1 \cong 1.3$ Å^{-1} in wide-angle X-ray scattering measurements of Narten and Habenschuss[11,31] on polyethylene melts.

Figure 7 depicts the partial structure factors computed for the vinyl chain melt for the case when $d_A = d_B = d_C = 1.0$ Å. Note that in the $k = 0$ limit all the partial structure factors reduce to the same value $\tilde{\rho}\hat{S}_{\alpha\gamma}(0) = \tilde{\rho}^2 k_B T\kappa = 0.1039$ dictated by the isothermal compressibility κ. At higher wave vectors each of the partial structure factors exhibits a different and complex behavior. In general, it is difficult to independently measure each of the scattering functions. The intensity $I(k)$ that is measured in a typical scattering experiment consists of a weighted sum of the individual partial structure factors

$$I(k) = \sum_{m,m'} b_m b_{m'} \hat{S}_{mm'}(k) \tag{15}$$

where b_m is the scattering cross section of the mth site.

In order to make comparisons with $I(k)$, in this investigation we define an average structure factor $\hat{S}_{site}(k)$ according to

$$\hat{S}_{site}(k) = \frac{1}{9}\sum_{m,m'} \hat{S}_{mm'}(k) \tag{16}$$

That is, we assume that the scattering cross sections of

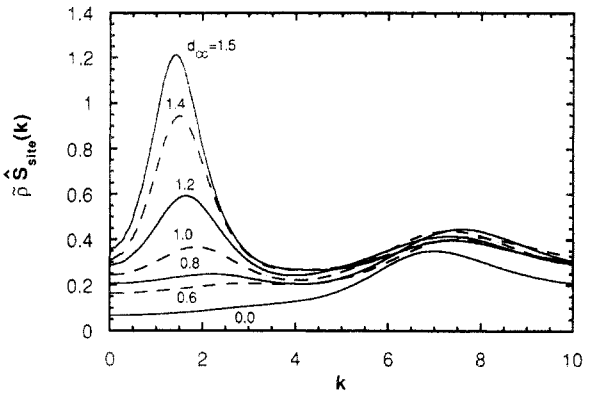

Figure 8. Average structure factor per site calculated from eq 16 as a function of wave vector k (Å^{-1}). The curves are shown for various values of the side-chain site diameter d_{CC} (Å). The backbone site diameters were $d_{AA} = d_{BB} = 1.0$ Å.

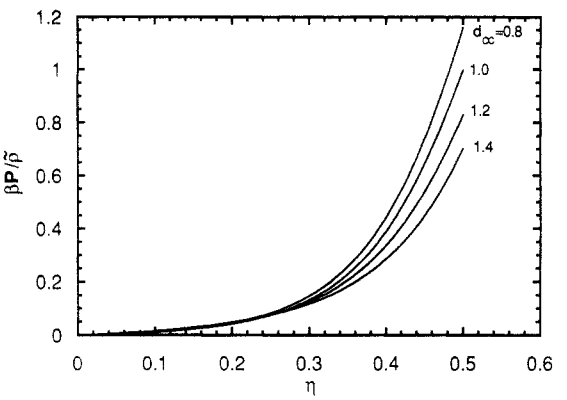

Figure 9. Pressure computed from the compressibility as a function of the packing fraction η. The curves are shown for various values of the side-chain site diameter d_{CC} (Å). The backbone site diameters were $d_{AA} = d_{BB} = 1.0$ Å. β is defined as $1/k_BT$ where k_B is Boltzmann's constant.

each of the three sites are equal. This average structure factor is plotted in Figure 8 for various side-chain site diameters d_{CC}. It is interesting to observe from this figure that a new peak grows at small wave vector when a side-chain site is added to a PE type backbone. This new peak grows in intensity and shifts to lower wave vectors as d_{CC} increases. For the case of $d_{CC} = 1.0$ Å, the low-angle peak occurs at $k_2 = 1.8$ corresponding to a characteristic distance of roughly $2\pi/k_2 \cong 3.5$. Such a low-angle peak, at wave vectors below the main peak, has been observed in amorphous polystyrene.[32] It is clear from examining Figure 7 that this peak in $\hat{S}_{site}(k)$ arises from the AA, BB, and AB partial structure factors corresponding to the backbone sites. These long-range backbone correlations must result from packing which is influenced by the side-chain sites. Thus, the side-chain sites indirectly account for the new low-angle peak by influencing the packing of the backbone sites.

V. Thermodynamic Properties

In principle, thermodynamic properties can be deduced from a knowledge of the intermolecular structure as given by the radial distribution functions. In the case of a polymer melt, the thermodynamic properties of interest include the isothermal compressibility κ, the equation-of-state, and the cohesive or internal energy E. The compressibility is easily obtained from the zero wave vector structure factor according to $\hat{S}_{mm'}(0) = \tilde{\rho}k_BT\kappa$. The pressure can then be obtained by integration of the compressibility

$$\frac{P}{\tilde{\rho}k_BT} = \frac{1}{\tilde{\rho}}\int_0^{\tilde{\rho}} \frac{d\rho}{\hat{S}_{mm'}(0)} \tag{17}$$

The pressure can also be computed from other routes. It should be mentioned that previous studies[12] on polymer melts demonstrate that different results are obtained from PRISM theory depending on which route is employed. Figure 9 shows the dependence of the pressure calculated in this manner as a function of the packing fraction. Note that, at a given packing fraction, the pressure decreases as the side-chain site diameter d_{CC} increases. Conversely, at fixed pressure the density of freely-jointed vinyl chain melts is predicted to increase with increasing side-chain diameter. Experimentally, the density of isotactic polypropylene is very slightly larger than for polyethylene.[33] Such a comparison between freely-jointed chain liquids and experimental densities on real polymer melts could be misleading, however, since the local intramolecular structure will strongly influence the intermolecular packing.

It is interesting to calculate the cohesive energy per site E for the vinyl polymer melt under investigation here becaue it is akin to the heat of mixing and enthalpic χ parameter[16] of a polymer blend. For a vinyl polymer melt, E is simply related to the radial distribution functions between sites A, B, and C according to the relation

$$E = \frac{1}{9}\sum_{m,m'}\int v_{mm'}(r)\, g_{mm'}(r)\, d\vec{r} \tag{18}$$

where $v_{mm'}(r)$ is the intersite potential. Previous work[5,29] on atomic and small-molecule fluids demonstrates that, at typical liquidlike densities, the radical distribution functions are determined almost entirely by the repulsive interactions. With this approximation, we can then employ the hard-core values of $g_{mm'}(r)$ in eq 18. For simplicity we assume that the intersite potentials outside the hard cores are of the Lennard-Jones form with equal well depths.

$$v_{mm'}(r) = \infty \quad \text{for } r < d_{mm'}$$

$$v_{mm'}(r) = 4\epsilon\left[\left(\frac{d_{mm'}}{r}\right)^{12} - \left(\frac{d_{mm'}}{r}\right)^{6}\right] \quad \text{for } r > d_{mm'} \tag{19}$$

Equation 18 is easily seen to reduce to

$$\frac{E}{16\pi\epsilon} = \frac{1}{9}\sum_{m,m'}\int_{d_{mm'}}^{\infty} r^2\, dr\left[\left(\frac{d_{mm'}}{r}\right)^{12} - \left(\frac{d_{mm'}}{r}\right)^{6}\right] g_{mm'}(r) \tag{20}$$

The cohesive energy is plotted in Figure 10 where it can be observed that E decreases as the side-chain site diameter d_{CC} increases. It is interesting to compare the cohesive energy per site of a freely-joined chain melt with the corresponding freely-joined polyethylene at the same packing fraction, size, and number of backbone sites. Correcting for the number of sites (four) per monomer, we find that $E/16\pi\epsilon = -0.149$ for polyethylene and -0.110 for the vinyl polymer with $d_{CC} = 1.0$ Å. This decrease in E for the polyethylene melt presumably reflects the fact that the unbranched chains are able to pack more efficiently than the vinyl chains at the same packing fraction. Since E is seen to be a sensitive function of the local structural details, one can speculate that the enthalpic χ parameter of a polymer blend would also depend on the local monomer structue and packing.[16] Furthermore, one would expect this dependence even when the site–site attractive potentials are identical.

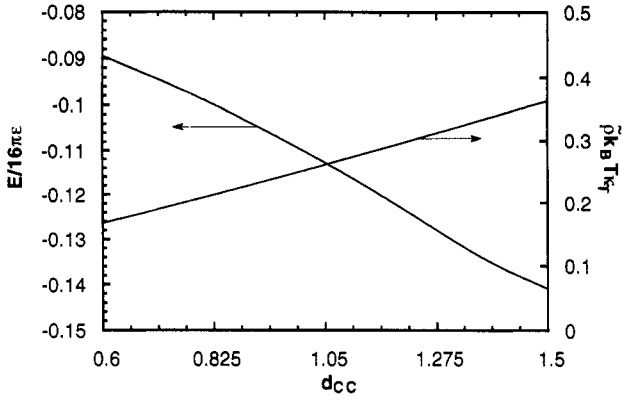

Figure 10. Cohesive or internal energy E per site (shown on the left-hand ordinate), and the isothermal compressibility (shown on the right-hand ordinate), as a function of the side-chain site diameter d_{CC} (Å). The backbone site diameters were $d_{AA} = d_{BB} = 1.0$ Å.

From Figure 10 it can be observed that the isothermal compressibility increases with d_{CC}. Again one might expect this trend to $d_{CC} > 0.6$ Å because the insertion of the side-chain group would be expected to disrupt the packing of the main chains, thereby raising the "free volume" and hence the compressibility. Experimentally, it appears that isotactic polypropylene melts have a slightly larger compressibility than polyethylene melts at the same temperature.[33] PRISM calculations, in which the local monomer structure is modeled with a rotational isomeric state model, are required to make a more definitive comparison between polyethylene and polypropylene.

VI. Conclusions

In this investigation we have calculated the intermolecular packing of freely-jointed, polymer melts. The effect of local monomer structure is captured by subdividing each monomer into three independent, tangent, hard-sphere sites. Not surprisingly, the local monomer structure influences the radial distribution functions on short length scales. Significant shielding of the backbone sites by the side-chain groups is observed when $d_{CC} > 0.6$ Å. In the range $0 \le r \le 0.4$ Å the flexible side-chain sites appear to pack efficiently between the larger backbone sites. On larger length scales comparable to the radius of gyration, all the radial distribution functions exhibit universal behavior characteristic of the correlation hole. This suggests that simpler coarse-grained models would suffice if one is interested only in long-range correlations.

Examination of the partial structure factors reveals that a new, low-angle peak, not present in polyethylene-like melts, emerges for vinyl polymers. This peak increases in intensity and moves to lower angles as the size of the side-chain group increases. Experimental evidence for this behavior possibly exists from X-ray scattering experiments on polystyrene melts. The results from the present investigation would suggest that this low-angle scattering behavior might be a general feature of vinyl polymer melts.

Thermodynamic properties deduced from the intermolecular radial distribution functions were found to be functions of the local monomer structure. Such nonuniversal behavior is expected since thermodynamic properties are known to depend on interchain correlations on all length scales. Calculations of intermolecular structure and thermodynamic properties for specific vinyl polymers are possible by employing the rotational isomeric state model to compute the intramolecular Ω functions in eq 6. Such calculations will be the topic of future investigations.

Acknowledgment. The author thanks Drs. K. S. Schweizer, J. D. McCoy, G. D. Wignall, and A. Habenschuss for helpful discussions regarding this investigation.

Appendix

In section III we estimated the fraction Δ of intramolecular overlaps of a freely-jointed chain. Here we outline the details of that straightforward, but tedious, computation. The overlap volume $V_{\alpha\gamma}(r)$ between two spheres a distance r apart having diameters $d_{\alpha\alpha}$ and $d_{\gamma\gamma}$ can be shown to be

$$\frac{rV_{\alpha\gamma}(r)}{d_{\alpha\gamma}^4} = \frac{\pi}{12}\left[\left(\frac{r}{d_{\alpha\gamma}}\right)^4 - 1.5\left(\frac{r}{d_{\alpha\gamma}}\right)^2\left(\frac{d_{\alpha\alpha}^2 + d_{\beta\beta}^2}{d_{\alpha\beta}^2}\right) + \left(\frac{r}{d_{\alpha\gamma}}\right)\left(\frac{d_{\alpha\alpha}^3 + d_{\beta\beta}^3}{d_{\alpha\beta}^3}\right) - \frac{3}{16}\left(\frac{d_{\alpha\alpha}^4 + d_{\beta\beta}^4}{d_{\alpha\beta}^4}\right) + \frac{3}{8}\left(\frac{d_{\alpha\alpha}}{d_{\alpha\beta}}\right)^2\left(\frac{d_{\beta\beta}}{d_{\alpha\beta}}\right)^2\right] \quad \text{(A1)}$$

The overlap fraction in eq 12 is based on the approximation that the total volume of overlap V_0 is the sum of pairwise overlaps. Thus, the simultaneous overlap of three or more spherical sites is neglected. Detailed analysis of eq 12, similar to that performed in ref 8 for single-site models, leads to the following expression for V_0

$$V_0 = \frac{1}{\pi}\int_0^\infty k\,dk \sum_{mm'} \hat{W}_{mm'}(k)\,\hat{G}_{mm'}(k) \quad \text{(A2)}$$

where the summation is over species A, B, and C. The $\hat{W}_{mm'}$ functions in eq A2 are related to intramolecular structure factors in eqs 9 and 10 but are modified by subtracting out the self terms when $m = m'$.

$$\hat{W}_{AA}(k) = \hat{W}_{BB}(k) = \frac{N}{2}(\hat{\Omega}_{AA} - 1) \quad \text{(A3a)}$$

$$\hat{W}_{CC}(k) = f_{BC}^2\hat{W}_{BB}(k); \quad \hat{W}_{AB}(k) = N\hat{\Omega}_{AB} \quad \text{(A3b)}$$

$$\hat{W}_{AC}(k) = f_{BC}\hat{W}_{AB}(k); \quad \hat{W}_{BC}(k) = f_{BC}\hat{W}_{BB}(k) \quad \text{(A3c)}$$

The $\hat{G}_{mm'}$ functions in eq A2 are related to the Fourier transform of the overlap volume of two spheres in eq A1.

$$\hat{G}_{mm'}(k) = \frac{\pi d_{mm'}^2 d_{mm}^2}{6} I_0(\xi_{mm'},kd_{mm'}) - 1.5D_2[I_2(1,kd_{mm'}) - I_2(\xi_{mm'},kd_{mm'})] + D_3[I_1(1,kd_{mm'}) - I_1(\xi_{mm'},kd_{mm'})] + \left[\frac{3}{8}\left(\frac{d_{mm}}{d_{mm'}}\right)^2\left(\frac{d_{m'm'}}{d_{mm'}}\right)^2 - \frac{3}{16}D_4\right][I_0(1,kd_{mm'}) - I_0(\xi_{mm'},kd_{mm'})] + \frac{\pi d_{mm'}^5}{12}[I_4(1,kd_{mm'}) - I_4(\xi_{mm'},kd_{mm'})] \quad \text{(A4)}$$

where $\xi_{mm'}$ and D_n are defined according to

$$\xi_{mm'} = \left|\frac{d_{m'm'} - d_{mm}}{2d_{mm'}}\right| \quad \text{and} \quad D_n = \frac{d_{mm}^n + d_{m'm'}^n}{d_{mm}^n}$$

In eq A4 it is assumed that $d_{m'm'} > d_{mm}$. If the opposite is true, then the coefficient of the first term on the right-hand side becomes $\pi d_{mm}^2 d_{m'm'}^2/6$ instead. The functions $I_n(\xi,kd)$ appearing in eq A4 are defined as

$$I_n(\xi,kd) = \frac{n!\cos\left(\frac{n\pi}{2}\right)}{(kd)^{n+1}} - \sum_{i=0}^{n} \frac{n!}{(n-i)!}\frac{\xi^{n-i}}{(kd)^{i+1}}\cos\left(kd\xi + \frac{\pi i}{2}\right) \quad \text{(A5)}$$

The desired overlap fraction Δ is now computed from eqs A1–A5 according to

$$\Delta = \frac{6V_0}{N\pi(d_{AA}{}^3 + d_{BB}{}^3 + d_{CC}{}^3)} \quad \text{(A6)}$$

The overlap fractions described in Table 1 were computed using eqs A1–A6.

References and Notes

(1) Schweizer, K, S.; Curro, J. G. *Phys. Rev. Lett.* **1987**, *58*, 246.
(2) Curro, J. G.; Schweizer, K. S. *Macromolecules* **1987**, *20*, 1928.
(3) Curro, J. G.; Schweizer, K. S. *J. Chem. Phys.* **1987**, *87*, 1842.
(4) Chandler, D.; Andersen, H. C. *J. Chem. Phys.* **1972**, *57*, 1930.
(5) Chandler, D. In *Studies in Statistical Mechanics VIII*; Montroll, E. W., Lebowitz, J. L., Eds.; North-Holland: Amsterdam, The Netherlands, 1982.
(6) Lowden, L. J.; Chandler, D. *J. Chem. Phys.* **1974**, *61*, 5228; **1973**, *59*, 6587; **1975**, *62*, 4246.
(7) Chandler, D.; Hsu, C. S.; Streett, W. B. *J. Chem. Phys.* **1977**, *66*, 5231. Sandler, S. I.; Narten, A. H. *Mol. Phys.* **1976**, *32*, 1543. Narten, A. H. *J. Chem. Phys.* **1977**, *67*, 2102. Hsu, C. S.; Chandler, D. *Mol. Phys.* **1978**, *36*, 215; *Mol. Phys.* **1979**, *37*, 299.
(8) Schweizer, K. S.; Curro, J. G. *Macromolecules* **1988**, *21*, 3070. Schweizer, K. S.; Curro, J. G. *Macromolecules* **1988**, *21*, 3082.
(9) Curro, J. G.; Schweizer, K. S.; Grest, G. S.; Kremer, K. *J. Chem. Phys.* **1989**, *91*, 1357.
(10) Honnell, K. G.; Curro, J. G.; Schweizer, K. S. *Macromolecules* **1990**, *23*, 3496.
(11) Honnell, K. G.; McCoy, J. D.; Curro, J. G.; Schweizer, K. S.; Narten, A. H.; Habenschuss, A. *J. Chem. Phys.* **1991**, *94*, 4659. Narten, A. H.; Habenschuss, A.; Honnell, K. G.; McCoy, J. D.; Curro, J. G.; Schweizer, K. S. *J. Chem. Soc., Faraday Trans.* **1992**, *88*, 1791.
(12) Yethiraj, A.; Curro, J. G.; Schweizer, K. S.; McCoy, J. D. *J. Chem. Phys.* **1993**, *98*, 1635. Curro, J. G.; Yethiraj, A.; Schweizer, K. S.; McCoy, J. D.; Honnell, K. G. *Macromolecules* **1993**, *26*, 2655.
(13) Schweizer, K. S.; Curro, J. G. *Chem. Phys.* **1990**, *149*, 105. Schweizer, K. S.; Curro, J. G. *J. Chem. Phys.* **1991**, *94*, 3986.
(14) Schweizer, K. S.; Curro, J. G. *Phys. Rev. Lett.* **1988**, *60*, 809. Curro, J. G.; Schweizer, K. S. *J. Chem. Phys.* **1988**, *88*, 7242.
(15) Schweizer, K. S.; Curro, J. G. *J. Chem. Phys.* **1989**, *91*, 5059. Curro, J. G.; Schweizer, K. S. *Macromolecules* **1990**, *23*, 1402. Curro, J. G.; Schweizer, K. S. *Macromolecules* **1991**, *24*, 6736.
(16) Schweizer, K. S.; Yethiraj, A. *J. Chem. Phys.* **1993**, *98*, 9053. Yethiraj, A.; Schweizer, K. S. *J. Chem. Phys.* **1993**, *98*, 9080. Yethiraj, A.; Schweizer, K. S. *J. Chem. Phys.* **1992**, *97*, 1455. Yethiraj, A.; Schweizer, K. S. *J. Chem. Phys.* **1992**, *97*, 5927. Schweizer, K. S. *Macromolecules* **1993**, *26*, 6033; *Macromolecules* **1993**, *26*, 6050.
(17) David, E. F.; Schweizer, K. S. *J. Chem. Phys.* **1994**, *100*, 7767.
(18) Flory, P. J. *J. Chem. Phys.* **1949**, *17*, 203.
(19) Ballard, D. G.; Schelton, J.; Wignall, G. D. *Eur. Polym. J.* **1973**, *9*, 965.
(20) Cotton, J. P.; Decker, D.; Benoit, H.; Farnoux, B.; Higgins, J.; Jannick, G.; Ober, R.; Picot, C.; des Cloizeaux, J. *Macromolecules* **1974**, *7*, 863.
(21) Curro, J. G. *J. Chem. Phys.* **1976**, *64*, 2496; *Macromolecules* **1979**, *12*, 463.
(22) Vacatello, M.; Avitabile, G.; Corradini, P.; Tuzi, A. *J. Chem. Phys.* **1980**, *73*, 543.
(23) Schweizer, K. S.; Honnell, K. G.; Curro, J. G. *J. Chem. Phys.* **1992**, *96*, 3211.
(24) Melenkevitz, J.; Curro, J. G.; Schweizer, K. S. *J. Chem. Phys.* **1993**, *99*, 5571.
(25) Melenkevitz, J.; Schweizer, K. S.; Curro, J. G. *Macromolecules* **1993**, *26*, 6190.
(26) Grayce, C. J.; Schweizer, K. S. *J. Chem. Phys.* **1994**, *100*, 6846.
(27) Grayce, C. J.; Yethiraj, A.; Schweizer, K. S. *J. Chem. Phys.* **1994**, *100*, 6857.
(28) Yamakawa, H. *Modern Theory of Polymer Solutions*; Harper & Row: New York, 1971.
(29) Hansen, J. P.; McDonald, I. R. *Theory of Simple Liquids*, 2nd ed.; Academic Press: London, 1986.
(30) de Gennes, P.-G. *Scaling Concepts in Polymer Physics*; Cornell University Press: Ithaca, NY, 1979.
(31) Narten, A. H. *J. Chem. Phys.* **1989**, *90*, 5857.
(32) Mitchell, G. R.; Windle, A. H. *Polymer* **1984**, *25*, 906.
(33) Zoller, P. *J. Appl. Polym. Sci.* **1979**, *23*, 1057.